

Spin-orbit-coupled fractional oscillators and trapped Bose-Einstein condensates

V. A. Stephanovich , E. V. Kirichenko , G. Engel , and A. Sinner 
Institute of Physics, University of Opole, Oleska 48, 45-052, Opole, Poland

 (Received 14 August 2023; accepted 4 January 2024; published 22 January 2024)

We study the ensemble of pseudo-spin 1/2 ultracold bosons, performing Lévy flights, confined in a parabolic potential. The (pseudo-) spin-orbit coupling (SOC) is additionally imposed on these particles. We consider the structure and dynamics of macroscopic pseudospin qubits based on Bose-Einstein condensates, obtained from the above “fractional” bosons. Under “fractional” we understand the substitution of the ordinary second derivative (kinetic energy term) in the Gross-Pitaevskii equation by a so-called fractional Laplacian, characterized by the Lévy index μ . We show that the joint action of interparticle interaction, SOC, and Zeeman splitting in a synthetic magnetic field makes the dynamics of corresponding qubit highly nontrivial with evident chaotic features at both strong interactions and Lévy indices $\mu \rightarrow 1$ when the Lévy trajectories of bosons with long jumps dominated over those derived from ordinary Gaussian distribution, corresponding to $\mu = 2$. Using analytical and numerical arguments, we discuss the possibilities to control the above qubit using the synergy of SOC, interaction strength, and “fractionality,” characterized by the Lévy index μ .

DOI: [10.1103/PhysRevE.109.014222](https://doi.org/10.1103/PhysRevE.109.014222)

I. INTRODUCTION

The importance of Bose-Einstein condensation lies in its profound implications in many branches of physics [1,2]. For instance, its microscopic properties are important for the description of many unusual phenomena in condensed matter systems. This is especially true for spin-orbit coupled Bose-Einstein condensates (BECs) [1], which could serve as the model object for topological insulators [3,4], spintronic devices [5], and spin-Hall effect [3,4,6,7]. As the formation of a BEC is an example of a phase transition, where the statistics of the individual boson trajectories play a more important role than boson-boson interaction, the former statistics is extremely important. The usual description of such statistics [2] is based on Gaussian elementary trajectories and is well studied.

Here we are concerned with the non-Gaussian statistics of underlying bosons. To be specific, we consider the possibility of bosons to perform so-called Lévy flights [8]. A Lévy flight is a Markovian random process, characterized by occasional long jumps or flights, which result in so-called heavy-tailed (i.e., non-Gaussian) probability distributions. Such a process involves particle movements that deviate significantly from a standard Brownian motion. In Lévy flights, the probability density function (pdf) follows a Lévy stable law [8–10]. A stable probability distribution is one that preserves its shape under convolution, making it a suitable candidate for modeling phenomena with non-Gaussian pdfs and irregular behavior [8–10]. The index parameter μ in the range of $0 < \mu < 2$ determines the stability of the Lévy flight, with lower values indicating more significant fluctuations in the particle’s trajectory. The case $\mu = 2$ corresponds to Gaussian pdf.

Fractional derivatives have emerged as a widely accepted approach for describing non-Gaussian phenomena; see [11,12] and references therein. These derivatives are particularly notable for their ability to generate the above Lévy stable pdfs in both spatial and temporal contexts [9,10,13].

They have found widespread use in characterizing the non-Gaussian properties observed in a corps of physical, chemical, biological, and financial systems [13–17]. Another important application of Lévy processes is in fractional quantum mechanics [18], dealing with the substitution of the ordinary Laplacian with the fractional one in the corresponding stationary Schrödinger equation. In the one-dimensional case, the definition of the fractional Laplacian reads

$$|\Delta|^{\mu/2} f(x) = -A_{\mu} \int \frac{f(u) - f(x)}{|u - x|^{\mu+1}} du, \quad (1)$$

$$A_{\mu} = \frac{\Gamma(1 + \mu)}{\pi} \sin \frac{\pi \mu}{2}. \quad (2)$$

Here $\Gamma(x)$ is the Γ function [19]. The operator (1) is spatially nonlocal with a slowly decaying power-law kernel (dictated by the Lévy index) typical for memory effects in complex disordered systems.

We note in this context that the Laskin construction of the fractional quantum mechanics [18] is based on the path integral over Lévy (i.e., a kind of Lévy flight) quantum mechanical trajectories. This procedure is qualitatively similar to the Feynman path integral, which is taken over Brownian particle trajectories. Evaluation of the path integral over Brownian trajectories generates the “ordinary” Schrödinger equation, while that over Lévy trajectories generates the fractional Schrödinger equation [18]. That being said, here we have an analogy between the Langevin stochastic differential equation, which describes each (stochastic) elementary trajectory, and the corresponding Fokker-Planck one, which describes the (Gaussian in that case) pdf of the underlying trajectories. In the majority of cases (like solids), the application of both ordinary and fractional quantum mechanics does not require the explicit use of the above (classical) elementary trajectories. Rather, what is needed is the spectrum of corresponding (ordinary or fractional) Schrödinger equation. In quantum gases, contrary to solids, we can in principle trace

and control (using magnetic and/or laser fields in corresponding traps; see also below) the above elementary trajectories. In that sense hereafter we use the classical notion of trajectories concurrently with the calculation of such “quantum” characteristics as eigenenergies and eigenvectors.

We note also that the qualitative role of the (pseudo) spin-orbit coupling (SOC) is a kind of self-interaction between the bosons, analogous to that in solids (like semiconductors), containing electrons with real physical spin [1,20,21]. In solids, this self-interaction is absent in single-electron problems like electrons in quantum dots [21] and for bosonic ensembles with pseudospin may serve as an additional (to the Gross-Pitaevsky term; see below) source of the nonlinearity, which influences the physical properties of the BEC. The self-interactive SOC character in electronic systems permits us to represent it as a certain gauge, which can be subsequently removed by gauge transformation. The corresponding general method had been proposed in Ref. [21]. However, in the case of fractional derivatives this method cannot be used as here we do not deal with second spatial derivatives. That is why we apply different methods of our problem solution.

A quantum bit (qubit) is the fundamental unit of quantum information. The key feature of qubits that makes quantum computing so powerful is their ability to exist in multiple states at once due to the principle of quantum superposition [22]. The pseudospin 1/2 of spin-orbit coupled BECs can well serve as such a qubit; see [20,23] for details. If additionally, the pseudospin 1/2 bosons, belonging to latter spin-orbit coupled BECs, can perform Lévy flights in their trap (i.e., to have long excursions with finite probability [8,13] inside the trap), the Lévy index can serve as a parameter which permits us to control the above qubit properties. This is because since in solids the different μ 's correspond to different degrees of intrinsic (i.e., uncontrollable by the external stimuli like laser field or magnetic field) system-related disorder, in BECs this index can be easily varied, for instance, by the above spatially dependent laser fields. To measure the qubit properties, the experimental techniques (permitting us to measure reliably the correlated motion of spin and coordinates), elaborated in Refs. [24–26], can be used.

In the present paper, we study the influence of underlying bosons Lévy trajectories on the properties of such “fractional” (in the above sense of substitution the ordinary kinetic energy term by the fractional Laplacian (1)) spin-orbit-coupled BECs. By varying the Lévy index μ , we can manipulate the corresponding “fractional qubit.” As our problem is closely related to the spectrum of the fractional quantum oscillator with spin-orbit coupling, in Sec. II we give an approximate analytical solution for this problem. The accuracy of this solution has been checked with direct numerical simulations. In Sec. III, within the Gross-Pitaevsky (GP) approach, we analyze the structure and dynamical properties of “fractional” [i.e., that with kinetic energy operator being substituted by a fractional Laplacian (1)] qubit, formed by SOC-coupled BECs with driven macroscopic qubits. Conclusions will be given in Sec. IV.

II. FRACTIONAL HARMONIC OSCILLATOR WITH SOC

Before studying the actual quasi-one-dimensional pseudospin 1/2 qubit dynamics, we consider the auxiliary

problem, which will be the base for our consideration. Namely, here we consider the spectrum of the 1D fractional harmonic oscillator with an additional SOC term. Below this problem will be augmented by the corresponding nonlinear Gross-Pitaevsky term, which accounts for the interaction between bosons in BEC. The Hamiltonian of our auxiliary problem reads in the coordinate space

$$\mathcal{H} = -\frac{1}{2}|\Delta|^{\mu/2} + \frac{x^2}{2} + \alpha\sigma_z p_x, \quad (3)$$

where $|\Delta|^{\mu/2}$ is determined by the expression (1) and σ_z is third Pauli matrix. Here we adopt the units $\hbar = \omega = m = 1$, where m and ω are the boson mass and the frequency of the trap (so that the oscillator length $l = \sqrt{\hbar/m\omega}$), respectively.

Also, here $p_x = -id/dx$ is the x component of the momentum operator so that the kinetic energy would be proportional to $|p_x|^\mu$ [18] rather than p_x^2 as in ordinary quantum mechanics. This is in accord with fractional Laplacian (1) properties, which at $\mu = 2$ gives ordinary Laplacian. Moreover, below we shall see that the transition to momentum space permits us to reduce the integral Schrödinger equation for the operator (3) to the differential one. The latter equation can be easily solved variationally as well as approximately (but with very good accuracy) reduced to the ordinary quantum harmonic oscillator problem. This will be done in the spirit of our previous results regarding fractional quantum oscillators [27].

The above is related to the well-known fact that integral (1) exists only in the sense of its Cauchy principal value [11,12]. This already complicates the solutions of spectral problems like (3) for integral operators [12]. Our analysis demonstrates that a more advantageous approach involves transitioning to the momentum space through Fourier transformation, where the operator (1) simplifies to $-|k|^\mu$. To obtain the eigenfunctions in coordinate space, we subsequently carry out the inverse Fourier transformation.

The explicit form of the Schrödinger equation for the components of spinor wave function

$$\Psi = \frac{1}{\sqrt{2}} \begin{pmatrix} \psi_\uparrow \\ \psi_\downarrow \end{pmatrix} \quad (4)$$

reads

$$\begin{aligned} -\frac{1}{2}|\Delta|^{\mu/2}\psi_\uparrow(x) + \frac{x^2}{2}\psi_\uparrow(x) + i\alpha\frac{d\psi_\uparrow}{dx} &= E\psi_\uparrow(x), \\ -\frac{1}{2}|\Delta|^{\mu/2}\psi_\downarrow(x) + \frac{x^2}{2}\psi_\downarrow(x) - i\alpha\frac{d\psi_\downarrow}{dx} &= E\psi_\downarrow(x), \end{aligned} \quad (5)$$

where E is an eigenenergy. As so far the problem is linear, there is no need to include the number of bosons N in the normalization of spinor (4). This normalization reads

$$\int_{-\infty}^{\infty} \Psi^\dagger(x)\Psi(x) dx = 1. \quad (6)$$

Now we apply Fourier transformation to both parts of Eqs. (5) to obtain

$$\begin{aligned} -\frac{1}{2}\psi_\uparrow''(k) + \left(\frac{1}{2}|k|^\mu + \alpha k\right)\psi_\uparrow(k) &= E\psi_\uparrow(k), \\ -\frac{1}{2}\psi_\downarrow''(k) + \left(\frac{1}{2}|k|^\mu - \alpha k\right)\psi_\downarrow(k) &= E\psi_\downarrow(k). \end{aligned} \quad (7)$$

Hence, in momentum space the Hamiltonian (3) converts to

$$\mathcal{H}_k = \frac{1}{2}|k|^\mu - \frac{1}{2} \frac{d^2}{dk^2} + \alpha k \sigma_z. \quad (8)$$

This shows that in momentum space we are essentially dealing with the “ordinary” (i.e., that with second derivative standing for kinetic energy) spin-orbit coupled quantum harmonic oscillator, but in the potential

$$U_\mu(k) = \frac{1}{2}|k|^\mu \pm \alpha k. \quad (9)$$

Although Eqs. (7) are simpler than the initial set (5), it is barely possible to analytically solve them, i.e., to calculate the energy spectrum and wave functions ψ_\uparrow and ψ_\downarrow for arbitrary $\mu < 2$. Therefore, in order to understand the energy spectrum and the corresponding eigenstates of the above problem, one has to rely on either approximate (like variational) or numerical methods.

To get more insights into the problem (7), we first consider the “ordinary” case $\mu = 2$. In this case the set (7) assumes the form

$$\begin{aligned} -\frac{1}{2}\psi_\uparrow''(k) + \left(\frac{1}{2}k^2 + \alpha k\right)\psi_\uparrow(k) &= E\psi_\uparrow(k), \\ -\frac{1}{2}\psi_\downarrow''(k) + \left(\frac{1}{2}k^2 - \alpha k\right)\psi_\downarrow(k) &= E\psi_\downarrow(k). \end{aligned} \quad (10)$$

Using the identical transformation of the potential

$$U_2(k) = \frac{1}{2}k^2 \pm \alpha k = \frac{1}{2}[(k \pm \alpha)^2 - \alpha^2], \quad (11)$$

we reduce the system (10) to the two almost identical equations for 1D quantum oscillators, which has a solution

$$\psi_\uparrow = \psi_n(k + \alpha), \quad \psi_\downarrow = \psi_n(k - \alpha), \quad (12)$$

$$E_n = n + \frac{1}{2} - \frac{\alpha^2}{2}, \quad (13)$$

where n labels the discrete states and $\psi_n(z)$ are ordinary oscillator wave functions (see, e.g., [28])

$$\psi_n(z) = e^{-z^2/2} \frac{H_n(z)}{\pi^{1/4} \sqrt{n! 2^n}}, \quad (14)$$

where $H_n(z)$ are Hermite polynomials of the n th order [19].

To better visualize the difference between the “ordinary” (11) and fractional (9) potentials, the latter is plotted in Fig. 1. Two distinct behaviors of potential $U_\mu(k)$ are reported in Figs. 1(a) and 1(b), respectively. Namely, if for $\alpha > 0.5$ (we take $\alpha = 0.6$ for concreteness), the minima of the potential go to infinities as $\mu \rightarrow 1$ [Fig. 1(a)], the situation in Fig. 1(b) ($\alpha = 0.4 < 0.5$) is opposite: the minima go to zero. To get into this situation, we find the point k_0 , where the potential $U_\mu(k)$ (9) has the minimum

$$k_0 = \pm \left(\frac{2\alpha}{\mu} \right)^{1/(\mu-1)}. \quad (15)$$

Expression (15) shows that at $\mu = 1$, the value k_0 goes either to zero or to infinity depending on whether 2α is greater or less than unity. More insights can be gained if we expand k_0 near its singular point $\mu = 1$. We have in this case

$$k_0(\mu \rightarrow 1) = \frac{1}{e} \exp\left(\frac{\ln 2\alpha}{\mu - 1}\right) \quad (16)$$

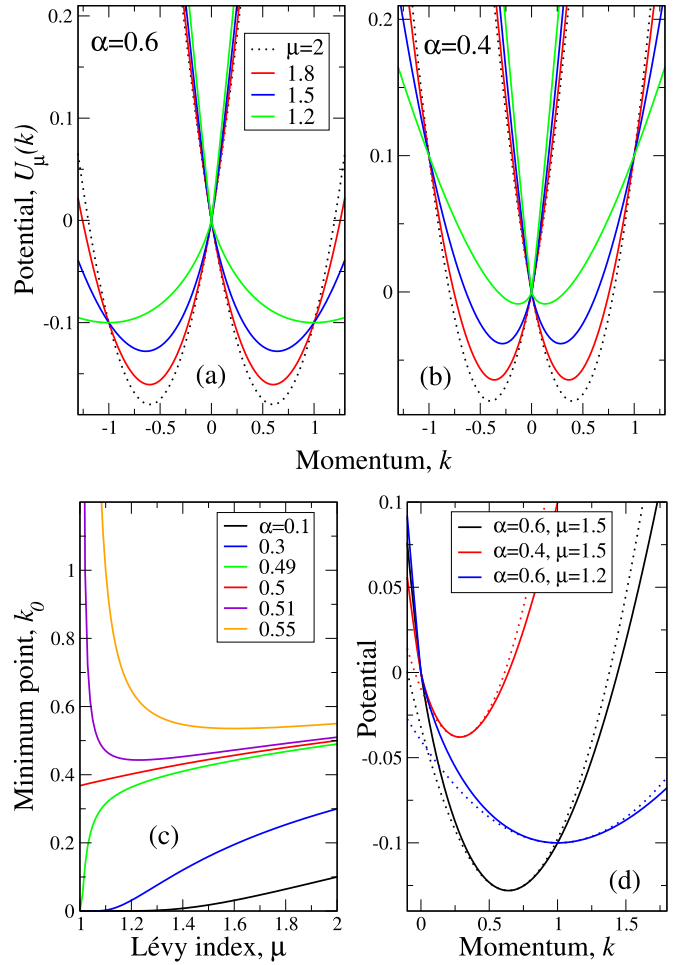


FIG. 1. (a) Potential $U_\mu(k)$ (9) for different Lévy indices μ , coded by colors and shown in the legend. The dotted line corresponds to the “ordinary” case $\mu = 2$, and solid lines to the case $\mu < 2$. (a) Case $\alpha > 0.5$ ($\alpha = 0.6$), when minimal point $k_0 \rightarrow \infty$ as $\mu \rightarrow 1$; (b) the opposite case $\alpha < 0.5$ ($\alpha = 0.4$), when $k_0 \rightarrow 0$ as $\mu \rightarrow 1$. The colors for different μ 's in (b) are the same as those in (a). (c) Minimum point k_0 as a function of the Lévy index μ . Values of SOC constant α are coded by colors and are shown in the legend. The curve for a special point $\alpha = 0.5$ (red), at which $k_0(\mu = 1) = 1/e$ ($e = 2.718\dots$ is the Euler number), separates two regimes, reported in (a) and (b). (d) Parabolic approximation (17) (dotted lines) of the potential $U_\mu(k)$ (9) (solid lines) for several selected μ and α values (legend).

($e = 2.71828\dots$ is the Euler number), which immediately demonstrates that $k_0(\mu \rightarrow 1) \rightarrow \infty$ at $\alpha > 0.5$, $k_0(\mu \rightarrow 1) \rightarrow 0$ at $\alpha < 0.5$ and $k_0(\mu \rightarrow 1) = 1/e \approx 0.3679$ at $\alpha = 0.5$. This behavior is reported in Fig. 1(c). Note that at $\mu = 2$ $k_0 = \pm\alpha$, which is in accord with “ordinary” behavior, given by the expressions (11)–(13). We note also that our numerical analysis (see below) shows that the solutions to our problem exist for Lévy indices $1 < \mu < 2$ only. Expression (15) actually confirms this point as $\mu = 1$ is a singularity.

The shape of potentials in Figs. 1(a) and 1(b) suggests the method of the approximate solution of our problem. Namely, the regions of $U_\mu(k)$ near minima can be well approximated by the parabolas. In this case, we can easily obtain the

approximate solution of the Schrödinger equations (7) in the spirit of expressions (11)–(13). The parabolic approximation of the potential $U_\mu(k)$ (9) can be obtained by its expansion in the Taylor series near the point k_0 (15). This gives for the right well ($k_0 > 0$)

$$\begin{aligned} U_\mu(k) &\approx U_0 + U_2(k - k_0)^2, \\ U_0 &= \frac{1 - \mu}{2} \left(\frac{2\alpha}{\mu} \right)^{\mu/(\mu-1)}, \\ U_2 &= \frac{\mu(\mu - 1)}{4} \left(\frac{2\alpha}{\mu} \right)^{(\mu-2)/(\mu-1)}. \end{aligned} \quad (17)$$

The above parabolic approximation for several selected curves $U_\mu(k)$ (also the right well; the approximation for the left well is the same) is shown in Fig. 1(d). It is seen that while the parabola is indistinguishable from the original curve near its minimum, the visible discrepancies begin approximately at “half width” of the potential curve near its minimum. This means that such a parabolic approximation is good to describe the ground and may be a couple of low-lying excited states. Our analysis shows that the errors more than 15% between the exact numerical and approximate spectrum start at the third excited state only. At $\mu > 1.7$ higher (then a third) excited states could also be described quantitatively. But apart for the above discrepancies for higher excited states, the above parabolic approximation gives good qualitative approximation of the entire spectrum. Below we shall see that this method being much less laborious than a variational approach [27] (see below) gives an even better approximation for the spectrum.

Substitution of the parabolic approximation (17) into the Schrödinger equations (7) generates the following approximate solution:

$$\begin{aligned} \psi_\uparrow &= \psi_n[(2U_2)^{1/4}(k + k_0)], \\ \psi_\downarrow &= \psi_n[(2U_2)^{1/4}(k - k_0)], \end{aligned} \quad (18)$$

$$E_n = U_0 + \sqrt{2U_2} \left(n + \frac{1}{2} \right), \quad (19)$$

where $\psi_n(z)$ are given by (14). Note that at $\mu = 2$ $U_0 = -\alpha^2/2$ and $U_2 = 1/2$ so that in this case we arrive at the “ordinary” expression for the spectrum (13). The same is valid for the states ψ_\uparrow and ψ_\downarrow .

Another method of approximate solution of the Schrödinger equations (7) is the variational approach [27]. It turns out that the asymptotics of wave functions in our case is similar to that of an ordinary (i.e., without SOC) fractional harmonic oscillator [27] $\psi(k \rightarrow \pm\infty) \sim \exp(a|k|^{1+\mu/2})$, $a = \text{const}$ [27]. This permits us to construct the trial functions $\psi_\uparrow = \psi_n(k + k_0)$, $\psi_\downarrow = \psi_n(k - k_0)$, where $n = 0, 1, 2, \dots$ enumerates the states of discrete spectrum, k_0 is defined by the expression (15), and

$$\begin{aligned} \psi_0(z) &= A_0 e^{-a_0|z|^{1+\mu/2}}, \quad \psi_1(z) = A_1 z e^{-a_1|z|^{1+\mu/2}}, \\ \psi_2(z) &= A_2 (1 + b_2 z^2) e^{-a_2|z|^{1+\mu/2}}, \dots \end{aligned} \quad (20)$$

Here a_i and b_i are variational parameters, while A_i are normalization coefficients. As we choose our spinor Ψ in the form (4), the normalization condition for the functions (20)

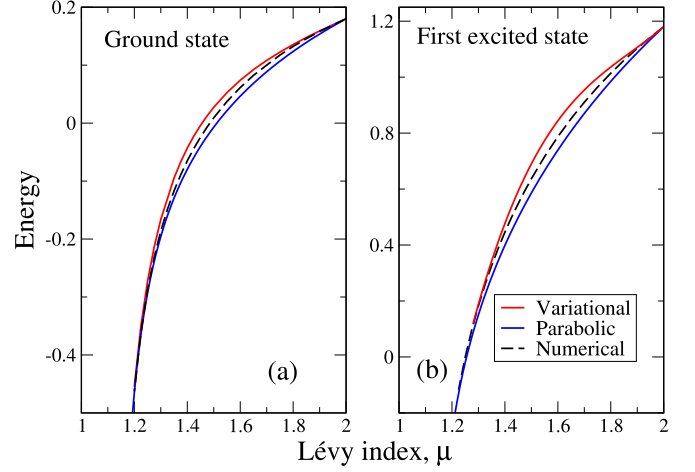


FIG. 2. Ground (a) and first excited (b) state energies vs Lévy index μ , calculated with three different methods. In both panels are reported the curves for SOC constant $\alpha = 0.8$; the curves for other α 's are qualitatively similar. For the Lévy index $\mu = 2$ (“ordinary case”), the energies have values 0.18 (ground state) and 1.18 (first excited state) following expression (13).

reads

$$\int_{-\infty}^{\infty} \psi_n^2(z) dz = 1. \quad (21)$$

This condition relates A_i to a_i and b_i , which are found both from the minimization of the energy

$$W_n = \int_{-\infty}^{\infty} \Psi^\dagger(x) \mathcal{H} \Psi(x) dx \quad (22)$$

and orthogonality conditions like $\int_{-\infty}^{\infty} \psi_1 \psi_0 dk = 0$, $\int_{-\infty}^{\infty} \psi_2 \psi_1 dk = 0$, etc.; see Ref. [27] for details. Here the spinor is defined by the expression (4) and the Hamiltonian \mathcal{H} by the expression (3). The above method permits us to construct the trial function for the whole discrete spectrum of our oscillator. Namely, each wave function (20) consists of the exponential factor multiplied by the polynomial with so far unknown coefficients. The order of the polynomial corresponds to the order of the energy state n and is dictated by the number of nodes which the wave function ψ_n should have (the so-called oscillation theorem; see, e.g., [28]). With respect to the above normalization and orthogonality conditions, this construction permits us to find the approximate spectrum of the problem by minimization of the functional (22). The comparison of the ground and first excited state energies as functions of the Lévy index μ are reported in Fig. 2. It is seen, that for both states, the variational curve goes higher than the exact, i.e., the numerical one. This reflects the well-known fact from the variational principle of quantum mechanics [28], which states that the true minimum of the energy is achieved for the exact solution only, while the variational method approaches this (true) minimum from above. It is also seen that at $\mu \rightarrow 1$ both ground and first excited state energy go to minus infinity, giving rise to the “infinite minimum” of the oscillator energy. Our analysis shows that such behavior occurs for higher excited states also. Moreover, as the energy at $\mu < 2$ lies below that for

$\mu = 2$, we can speculate that the Bose condensate with Lévy elementary trajectories is more energetically favorable (say, more stable) than that with normal, Gaussian ones. This fact should be taken into account while working, for instance with Bose condensate qubits; see also below. One more observation is in place here. Namely, as for ground state energy [Fig. 2(a)] both variational and “parabolic” [i.e., spectrum (19) obtained using parabolic approximation (17)] curves go approximately the same distance from the exact one, for the first excited state, the variational curve lies farther from the exact compared to the “parabolic” one. To be specific, while the maximal error for ground state energy is around 1.5% (between numerical and “parabolic” curves) and 2.1% (between numerical and variational curves), the same quantity for the first excited state is 5% and 7%, respectively. This means that in the problem of a spin-orbit coupled fractional quantum oscillator (say, linear fractional BEC qubit), the parabolic approximation, being much less laborious, than the variational one, gives a very good approximate solution to the problem.

III. DRIVEN FRACTIONAL QUANTUM BIT AND CHAOTIC RABI TRANSITIONS

A. Ground-state properties

The effective Hamiltonian, which we shall use to explore the development of the driven qubit, based on a quasi-one-dimensional pseudospin-1/2 spin-orbit coupled Bose condensate reads

$$\begin{aligned}
 \mathcal{H}_1 = & -\frac{1}{2}|\Delta|^{\mu/2} + \frac{[x - d(t)]^2}{2} + \alpha\sigma_z p_x \\
 & + \frac{1}{2}\delta\sigma_x + g_1|\Psi|^2.
 \end{aligned} \quad (23)$$

This Hamiltonian is obtained by adding the nonlinear (responsible for the interaction between bosons in BEC in the spirit of the GP approach [2]) and Zeeman terms to the initial linear Hamiltonian (3). Here $d(t)$ is the externally driven displacement of the harmonic trap center, δ is the synthetic Zeeman splitting [26], and $\sigma_{x,z}$ are the Pauli matrices. Note that the above external driving of the harmonic trap center can be accomplished through the gradual movement of the intersecting region of laser beams responsible for trapping the Bose condensate. Also, the dimensionless effective interaction constant $g_1 = 2\Omega_\perp L_s$, where $\Omega_\perp = \omega_\perp/\omega$ is dimensionless (in units of the parabolic trap frequency ω ; see above) transversal confinement frequency and $L_s = l_s/l$ is dimensionless (in units of the oscillator length l ; see also above) scattering length of interacting bosons [26]. Note that as $\omega_\perp \gg \omega$, parameters $\Omega_\perp > 10$ and $g_1 \sim 10^{-3}$ under a reasonable supposition $l_s \approx 100a_B$, where a_B is the Bohr radius. This means that the parameter $g_1 N$, responsible for the actual boson-boson interaction, will be around 50–100. In the spirit of the GP approach, the number of bosons N would now enter the normalization condition for spinor Ψ : $\int_{-\infty}^{\infty} \Psi^\dagger(x)\Psi(x) dx = N$. This implies that it is reasonable to choose $\Psi(x)$ in the form $\Psi(x) = \sqrt{N/2}(\psi_\uparrow, \psi_\downarrow)^T$ instead of (4). This, in turn, allows us to keep the normalization of ψ_\uparrow and ψ_\downarrow to unity.

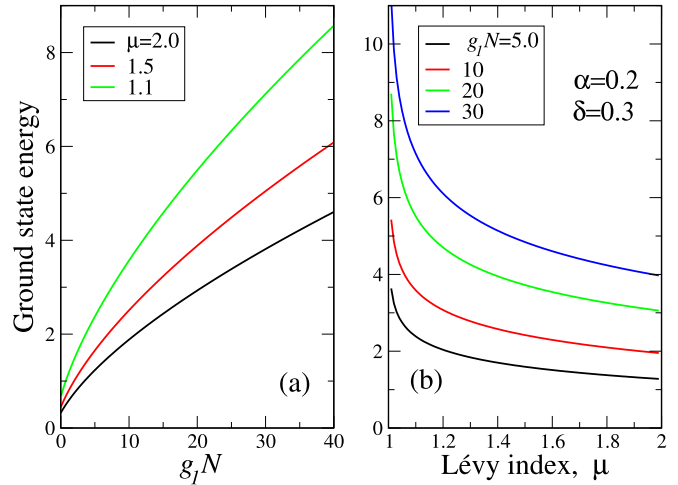


FIG. 3. BEC ground-state energy, calculated numerically at typical values $\alpha = 0.2$, $\delta = 0.3$. (a) Dependence on the interaction strength $g_1 N$ for three fixed Lévy indices μ , shown in the legend. (b) Dependence on μ at fixed $g_1 N$, also coded by colors and shown in the legend.

It is obvious that in the nonlinear case (23) the momentum space approach will not be any good so that here we should opt either to numerical methods or to variational ones. The above parabolic approximation can here be of good service too. Namely, the Fourier image of the “parabolic” ground state spinor wave function components (18)

$$\psi_{\uparrow,\downarrow,gs}(k) = \left(\frac{a}{\pi N^2}\right)^{1/4} \exp\left[-\frac{a}{2}(k \pm k_0)^2\right] \quad (24)$$

read in coordinate space

$$\psi_{\uparrow,\downarrow,gs}(x) = \left(\frac{N^2}{a\pi}\right)^{1/4} \exp\left[-\frac{x^2}{2a} \pm ik_0 x\right]. \quad (25)$$

Here we declare the coefficient $(2U_2)^{1/4}$ (18) as variational parameter a . It turns out that for $\mu \gtrsim 1.4$ the function (25) gives a fairly good approximation to the numerical solution of the problem. As $\mu \rightarrow 1$, the “cusps” at $x = 0$ and long tails at $x \rightarrow \pm\infty$, typical for systems with fractional derivatives, give the discrepancies between the exact numerical ground state wave function (to be more specific, the probability density $\Psi^\dagger\Psi$) and the variational one (25). But anyway, the trial function (25) delivers a good qualitative approximation for the BEC ground state for all admissible Lévy indices. Note that the trial function (25) contains phase factors $e^{ik_0 x}$, which stem from those related to SOC for the ordinary case $\mu = 2$ [23] as $k_0(\mu = 2) = \alpha$; see Eq. (15). This once more shows that in the fractional case we have one more possibility to control the properties of our BEC qubit by varying the Lévy index μ .

The numerical ground state energy is displayed in Fig. 3, where we plot the BEC ground state energy as a function of the interaction strength $g_1 N$ [Fig. 3(a)] and Lévy index μ [Fig. 3(b)]. It is seen from Fig. 3(a) that the ground state energy grows with an interaction parameter similar to the “ordinary” case of $\mu = 2$ [23]. Interestingly, contrary to the above linear case (i.e., that with $g_1 = 0$), the ground state energy grows as the Lévy index μ goes to unity. This is clearly visible in Fig. 3(b). This shows that in the nonlinear

case, the Lévy (say, chaotic; see Ref. [29] for pictorial representation) trajectories with long excursions are energetically unfavorable, giving rise to the ground state energy increase as compared to that in the Gaussian case $\mu = 2$. As our nonlinear BEC is indeed a soliton [30], we speculate here that the synergy between nonlinearity and fractional dimension gives the higher resulting (ground state) energy at a higher participation rate of the trajectories with (extremely at $\mu \rightarrow 1$) long excursions. In other words, as a soliton realizes the balance between nonlinearity and spatial dispersion (in our case not only fractional kinetic energy but also SOC), this equilibrium (say balanced) state has the higher energy at $\mu \rightarrow 1$. This may suggest that contrary to the above linear case, the higher “chaotization” of underlying bosons trajectories (determined by the Lévy index μ) creates negative feedback in the BEC soliton formation due to nonlinear effects, giving rise to its ground state energy increase. To get more insights in this effect (lowering of the ground state energy as $\mu \rightarrow 1$ in the linear case and its rising in nonlinear one), perturbative (with g_1N being a small parameter) calculations are necessary. We postpone the studies of this interesting effect to future publications.

B. Dynamics and chaotic Rabi transitions

The time evolution of our spinor wave function Ψ is acquired by the solution of the time-dependent nonlinear Schrödinger equation

$$i \frac{\partial \Psi}{\partial t} = \mathcal{H}_1 \Psi, \quad (26)$$

where the Hamiltonian \mathcal{H}_1 is given by Eq. (23). Now, to control the above spin qubit, the traps center is subjected to harmonic driving at the frequency equal to the Zeeman splitting:

$$d(t) = d_0 \sin(t\delta), \quad (27)$$

where d_0 is an arbitrary driving amplitude. In this case the Rabi frequency ω_R of the corresponding spin rotation is defined as $\omega_R = \alpha d_0 \delta$. If so, the ideal Rabi oscillations of the average spin component assume the form

$$\langle \sigma_x(t) \rangle \equiv \frac{1}{N} \int_{-\infty}^{\infty} \Psi^\dagger(x, t) \sigma_x \Psi(x, t) dx = \cos \omega_R t. \quad (28)$$

This equation is derived under the supposition of noninteracting condensate with $\delta \ll 1$ and $\alpha \ll 1$. We will see below that the dynamics of our driven qubit will be (sometimes very) different from the ideal law (28).

The numerical time evolution of the spin component $\langle \sigma_x(t) \rangle$ [see Eq. (28) for definition] is reported in Fig. 4. It is seen that the joint action of fractional dimension (dictated by the Lévy index μ) and repulsive interparticle interaction (parameter g_1N) not only gives substantial deviation from the ideal Rabi oscillations (28) but also leads to the chaotic features in the time dependence of $\langle \sigma_x(t) \rangle$. The latter features are especially visible for the strong couplings $g_1N = 10$ and 30. At the same time, in the fractional situation with $\mu = 1.8$ [Fig. 4(b)] even in the linear case $g_1N = 0$ (black solid curve), the deviation from the ideal Rabi curve is higher than that in the ordinary case, shown in Fig. 4(a). This shows that

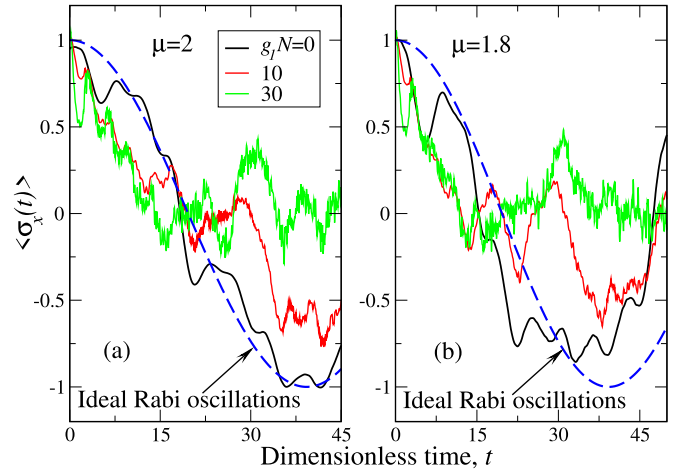


FIG. 4. Time evolution of the spin component $\langle \sigma_x \rangle$ for $\mu = 2$ (a) and $\mu = 1.8$ (b) at different interaction strengths g_1N , shown in the legend. Here $d_0 = 2.0$, $\alpha = 0.2$, and $\delta = 0.2$, which correspond to Rabi frequency $\omega_R = 0.08$. Ideal Rabi oscillations (28) are also shown.

irregular time dependence $\langle \sigma_x(t) \rangle$ can be primarily attributed to the (strong) repulsive interaction in the system. The irregular spin dynamics is also visible in Ref. [23], which means that the “fractionality” related to the admixture of individual bosons’ Lévy trajectories to the Gaussian ones enhances the chaotic features, which appear due to the nonlinearity in the system. Note that we have shown earlier [31,32] that in low-dimensional semiconductor systems with SOC, the chaotic behavior appears, in particular, due to SOC-generated nonlinearities in the equations of motion. Moreover, as has been demonstrated [31], the chaos appears at strong SOC, generating (also strong) nonlinear effects. This shows the qualitative similarity between spin dynamics in low-dimensional semiconductor structures with SOC and pseudospin dynamics of quasi-1D SOC-coupled BECs. It would be tempting to study the latter analogy in more detail, which not only would elucidate the synergy between SOC and fractional dimension in BEC but also may give more possibilities to drive and control the above BEC qubit. The main problem here is the transition from fractional quantum mechanics to its classical counterpart, namely, how the fractional kinetic energy operator $|\Delta|^{\mu/2}$ transforms to the correspondent classical quantity. The prescription is given in Ref. [18], where the former operator transforms to $|\dot{x}|^{\mu/(\mu-1)}$, where $\dot{x} = dx/dt$. This already makes the problem nonlinear, which suggests that the system may be prone to chaotic behavior. On the other hand, the solutions to such problem can be barely found analytically so that we should opt for numerical methods. This is especially true for the trajectory vector $\mathbf{Q}(t) = [x(t), \dot{x}(t)]$, which will subsequently be used to find the maximal Lyapunov exponent [32,33] to discern if the system is chaotic. We postpone the studies of these intriguing questions to future publications.

The above classical chaotic trajectories may find their quantum analog in the energy levels repulsion and other manifestations of the quantum chaos [34]. It would be also extremely useful to study the manifestations of quantum chaos

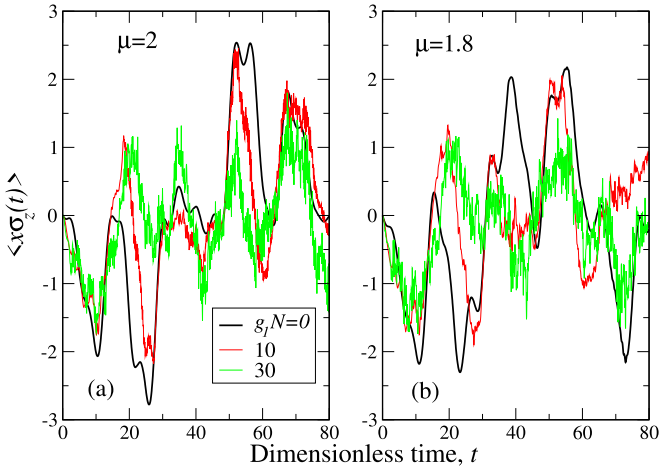


FIG. 5. Same as in Fig. 4 but for $\langle x\sigma_z(t) \rangle$. Interaction strengths are coded by colors and shown in the legend in (a). Here $d_0 = 2.0$, $\alpha = 0.2$, and $\delta = 0.2$.

both in our system and in solids with SOC in the context of fractional quantum mechanics [18].

Another important characteristic of our system is the spin density dipole moment $\langle x\sigma_z(t) \rangle$, which plays an important role in the driving of the above macroscopic qubit. It is defined analogously to $\langle \sigma_x(t) \rangle$ (28), and its time evolution is reported in Fig. 5. The same (as those in Fig. 4) chaotic features in time evolution are clearly seen at strong couplings. This shows the qualitative similarity between the dynamics of $\langle \sigma_x(t) \rangle$ and $\langle x\sigma_z(t) \rangle$ in our system. To better understand the role of “fractionalization,” in Fig. 6 we show the dynamics of both $\langle \sigma_x \rangle$ and $\langle x\sigma_z \rangle$ components at some (not very large) fixed $g_1N = 10$ and different Lévy indices. It can be seen that already irregular, chaotic dynamics, which occurs (due to interaction effects) in the ordinary case $\mu = 2$, only enhances as $\mu \rightarrow 1$. Namely, Fig. 6(a) shows that as μ goes to 1, the deviations from the ideal Rabi oscillations become progressively larger so that already at $\mu = 1.5$ the system dynamics does not resemble

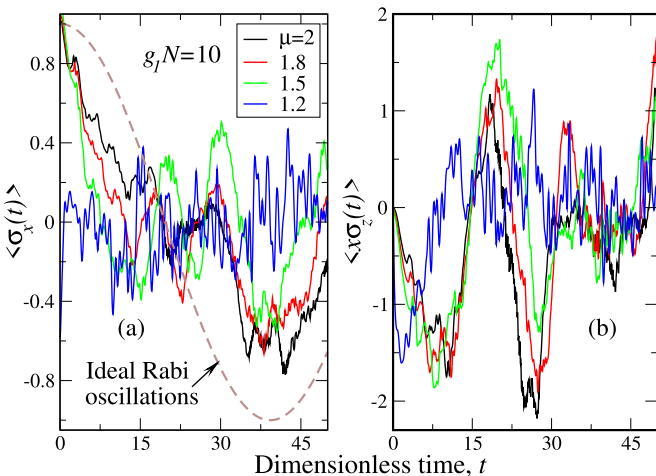


FIG. 6. Dynamics of $\langle \sigma_x(t) \rangle$ (a) and $\langle x\sigma_z(t) \rangle$ (b) at fixed $g_1N = 10$ and different Lévy indices μ , shown in the legend to (a). The parameters d_0 , α , and δ are similar to those in Figs. 4 and 5.

the oscillations (28). Also, at $\mu = 1.2$, the trajectories in both Fig. 6(a) and Fig. 6(b) resemble substantially some highly irregular, stochastic dynamics; i.e., we have very strong chaoticization. This shows that low Lévy indices play a similar role as strong interaction. In other words, even at moderate nonlinearities (i.e., interparticle interaction in the GP picture of BEC) but strong admixture of non-Gaussian, Lévy trajectories of each individual boson, we still arrive at the same irregular (say chaotic) dynamics. We pay attention here that the irregular time patterns in the curves in Figs. (4–6) have nothing to do with the classical chaotic trajectories. This is because they are obtained by the (numerical) solution of a time-dependent nonlinear Schrödinger equation (26), i.e., they are of a purely quantum nature. We call them “chaotic” here because they significantly resemble such trajectories. Once more, we postpone the detailed studies of the interplay between interaction strength g_1N and “fractionality,” characterized by the index μ for future publications.

IV. CONCLUSIONS AND OUTLOOK

When atoms of ultracold atomic gases perform Lévy flights, the probability for them to perform unbounded (and thus unpredictable) excursions may be close to unity. In this case it is barely possible not only to condense such atoms but also to control the properties of their BEC. To achieve the controllability of such BEC properties, it is necessary to “tame” the Lévy flight, i.e., to impose some constraints that prevent the extreme jumps or long-range excursions typically associated with a standard Lévy flight. In our case, such constraints are both the parabolic trap and interparticle interaction, modeled (within the GP approach) by the nonlinear term. In the present paper, using analytical and numerical arguments, we have shown that the macroscopic (quasi-) spin qubit, based on quasi-one-dimensional spin-orbit coupled BECs with fractional dispersion in a synthetic Zeeman magnetic field, has one more “degree of freedom,” which permits us to control its properties. This additional “degree of freedom” is Lévy index μ , which gives the measure of admixture of trajectories with long-range excursions to those of regular Brownian motion drawn from a Gaussian distribution. We have shown that in the linear case, without interaction, the fractional BEC qubit has smaller energy than that in the ordinary case, corresponding to $\mu = 2$. This means that the admixture of Lévy trajectories facilitates the formation of BEC and hence of the qubit. At the same time, if we “turn on” the repulsive interaction, its synergy with fractional dispersion gives the enhancement of BEC formed qubit energy already in the ground state. To be specific, it follows from Fig. 3 that the ground state energy grows at both interaction strength increase and at $\mu \rightarrow 1$, signifying more admixture of (very) long excursions to the individual particle trajectories. In other words, stronger interaction between particles, performing long jumps, plays a role of “destructive interference” for the collective behavior of these particles’ ensemble. One of the aims of the present work is to search for ways to convert the above “destructive interference” to the “amplifying” one, which would permit easier control of the BEC-formed qubit. The dynamics of harmonically driven qubit confirms the above conclusions. Namely, the irregular, chaotic features appear in the qubit dynamics.

In this case the high admixture of Lévy trajectories at $\mu \rightarrow 1$ plays the same role as high nonlinearity (strong interaction in the GP picture): the qubit motion becomes progressively more irregular and deviates substantially [in the case of $\langle \sigma_x(t) \rangle$] from the simple Rabi oscillations.

The present consideration also raised many questions, giving directions for future research. The first question is how to control experimentally the single-atom trajectories with the help of the Lévy index in BEC. It is well known [2] that the character of the above trajectories depends on the trap shape (parabolic, ring), the density of the atoms, and the presence of external stimuli like temperature, magnetic, and/or electric fields. Latter external fields comprise, in turn, the magnetic (magnetic fields) or optical (laser beams, creating so-called optical dipole potential) traps. In the above setups, different configurations of a magnetic and/or laser field generate different particle trajectories (and hence different wave functions, being the result of averaging over a multitude of the trajectories), which can well be of a Lévy type. In the latter case, to deduce the Lévy index from the experimental data, the best experimental technique might be time-of-flight (TOF) expansion (see [35] and references therein), which deals directly with the character of the BEC wave functions. To deduce the Lévy index from the TOF wave functions (density profiles), further work is needed to fit the above experimental density profiles by Lévy distributions.

It would be also interesting to trace perturbatively (at the small interaction strength $g_1 N$), how the decrease of the BEC ground state energy in the linear case transits into its increase in the nonlinear one. As nonlinearity generates the irregular, chaotic dynamics of the qubit's spin, this may shed light on the possibility to control the qubit time evolution by balancing the nonlinearity (interparticle interaction strength in GP picture) and fractional dimensions, characterized by the Lévy index

μ . Also, the methods used in Refs. [31,32] could be well applied to the detailed studies of possible chaotic dynamics of the above qubit. This might get more insights into the details of how the taming of Lévy flights by the parabolic potential permit one to overcome the detrimental effects caused by the repulsive interparticle interaction and actually SOC by itself. The latter fact, i.e., generation of chaotic dynamics by SOC, has been studied in Refs. [31,32]. The results of such studies might permit us to mitigate or completely avoid the undesirable chaotic behavior in the driven spin-qubit dynamics.

Another important question which should be studied is the quantum manifestations (like energy levels' repulsion and their non-Poissonian statistics [36]) of possible chaos in the dynamics of averaged spin components. This is because to date the quantum chaos [34,36] had been studied in the context of ordinary quantum mechanics, i.e., that with an ordinary Laplacian in the corresponding Schrödinger equation. We speculate that depending on the Lévy index μ the statistics of energy levels may vary in both the linear and nonlinear cases. This, in turn, may elucidate the above questions about quantum bit controllability from the "quantum side." Overall, as the physics of ultracold atomic SOC systems is very complex, further progress in the understanding of its intricate details is possible only when the theoretical results are supported by corresponding experimental findings.

ACKNOWLEDGMENTS

We are grateful to E. Ya. Sherman for illuminating discussions. We also acknowledge support of the Narodowe Centrum Nauki in Poland as research Project No. DEC-2017/27/B/ST3/02881 and of Grant No. JSF-22-10-0001 of the Julian Schwinger Foundation for Physics Research.

-
- [1] V. Galitski and I. B. Spielman, Spin-orbit coupling in quantum gases, *Nature (London)* **494**, 49 (2013).
 - [2] L. P. Pitaevsky and S. Stringari, *Bose-Einstein Condensation* (Clarendon Press, Oxford, 2003).
 - [3] D. Hsieh, D. Qian, L. Wray, Y. Xia, Y. S. Hor, R. J. Cava, and M. Z. Hasan, A topological Dirac insulator in a quantum spin Hall phase, *Nature (London)* **452**, 970 (2008).
 - [4] C. L. Kane and E. J. Mele, Z_2 topological order and the quantum spin Hall effect, *Phys. Rev. Lett.* **95**, 146802 (2005).
 - [5] J. D. Koralek, C. P. Weber, J. Orenstein, B. A. Bernevig, S.-C. Zhang, S. Mack, and D. D. Awschalom, Emergence of the persistent spin helix in semiconductor quantum wells, *Nature (London)* **458**, 610 (2009).
 - [6] Y. K. Kato, R. C. Myers, A. C. Gossard, and D. D. Awschalom, Observation of the spin Hall effect in semiconductors, *Science* **306**, 1910 (2004).
 - [7] M. König, S. Wiedmann, C. Brüne, A. Roth, H. Buhmann, L. W. Molenkamp, X.-L. Qi, S.-C. Zhang, Quantum spin Hall insulator state in HgTe quantum wells, *Science* **318**, 766 (2007).
 - [8] *Lévy Flights and Related Topics in Physics*, edited by M. F. Shlesinger, G. M. Zaslavsky, and U. Frisch, Lecture Notes in Physics Vol. 450 (Springer-Verlag, Berlin, 1995).
 - [9] P. Lévy, *Théorie de l'addition des Variables Aléatoires* (Gauthier-Villars, Paris, 1954).
 - [10] G. Samorodnitsky and M. S. Taqqu, *Stable Non-Gaussian Random Processes* (Chapman and Hall, New York, 1994).
 - [11] S. G. Samko, A. A. Kilbas, and O. I. Marichev, *Fractional Integrals and Derivatives* (Gordon and Breach, New York, 2003).
 - [12] I. Podlubny, *Fractional Differential Equations* (Academic Press, 1999).
 - [13] R. Metzler and J. Klafter, The restaurant at the end of the random walk: Recent developments in the description of anomalous transport by fractional dynamics, *J. Phys. A: Math. Gen.* **37**, R161 (2004).
 - [14] R. N. Mantegna and H. E. Stanley, *An Introduction to Econophysics, Correlations and Complexity in Finance* (Cambridge University Press, Cambridge, 2000).

- [15] S. Rachev, Y. Kim, M. Bianchi, and F. Fabozzi, *Financial Models with Lévy Processes and Volatility Clustering* (Wiley, New York, 2011).
- [16] G. M. Zaslavsky, *Hamiltonian Chaos and Fractional Dynamics* (Oxford University Press, New York, 2005).
- [17] R. Metzler, J.-H. Jeon, A. G. Cherstvy, and E. Barkai, Anomalous diffusion models and their properties: Non-stationarity, non-ergodicity, and ageing at the centenary of single particle tracking, *Phys. Chem. Chem. Phys.* **16**, 24128 (2014).
- [18] N. Laskin, *Fractional Quantum Mechanics* (World Scientific, Singapore, 2018).
- [19] M. Abramowitz and I. Stegun (eds.), *Handbook of Mathematical Functions* (Dover, New York, 1972).
- [20] T. D. Stanescu, B. Anderson, and V. M. Galitski, Spin-orbit coupled Bose-Einstein condensates, *Phys. Rev. A* **78**, 023616 (2008).
- [21] I. V. Tokatly and E. Ya. Sherman, Gauge theory approach for diffusive and precessional spin dynamics in a two-dimensional electron gas, *Ann. Phys.* **325**, 1104 (2010).
- [22] M. A. Nielsen and I. L. Chuang, *Quantum Computation and Quantum Information*, 2nd ed. (Cambridge University Press, Cambridge, 2010).
- [23] S. Mardonov, M. Modugno and E. Y. Sherman, Dynamics of a macroscopic spin qubit in spin-orbit coupled Bose-Einstein condensates, *J. Phys. B: At. Mol. Opt. Phys.* **48**, 115302 (2015).
- [24] J.-Y. Zhang, S.-C. Ji, Z. Chen, L. Zhang, Z.-D. Du, B. Yan, G.-S. Pan, B. Zhao, Y.-J. Deng, H. Zhai *et al.*, Collective dipole oscillations of a spin-orbit coupled Bose-Einstein condensate, *Phys. Rev. Lett.* **109**, 115301 (2012)
- [25] C. Qu, C. Hamner, M. Gong, C. Zhang, and P. Engels, Observation of *Zitterbewegung* in a spin-orbit-coupled Bose-Einstein condensate, *Phys. Rev. A* **88**, 021604(R) (2013).
- [26] Y.-J. Lin, K. Jiménez-García, and I. B. Spielman, Spin-orbit-coupled Bose-Einstein condensates, *Nature (London)* **471**, 83 (2011).
- [27] E. V. Kirichenko and V. A. Stephanovich, Confinement of Lévy flights in a parabolic potential and fractional quantum oscillator, *Phys. Rev. E* **98**, 052127 (2018).
- [28] L. D. Landau and E. M. Lifshits, *Quantum Mechanics. Nonrelativistic Theory* (Pergamon Press, Oxford, 1995).
- [29] D. Brockmann and I. M. Sokolov, Lévy flights in external force fields: From models to equations, *Chem. Phys.* **284**, 409 (2002).
- [30] H. Sakaguchi and B. A. Malomed, One- and two-dimensional solitons in spin-orbit-coupled Bose-Einstein condensates with fractional kinetic energy, *J. Phys. B: At. Mol. Opt. Phys.* **55**, 155301 (2022).
- [31] V. A. Stephanovich and E. Ya. Sherman, Chaotization of internal motion of excitons in ultrathin layers by spin-orbit coupling, *Phys. Chem. Chem. Phys.* **20**, 7836 (2018).
- [32] E. V. Kirichneko, V. A. Stephanovich, and E. Y. Sherman, Chaotic cyclotron and Hall trajectories due to spin-orbit coupling, *Ann. Phys. (Berlin)*, **532**, 2000012 (2020).
- [33] M. Cencini, F. Cecconi, and A. Vulpiani, *Chaos. From Simple Models to Complex Systems* (World Scientific, New Jersey, 2010).
- [34] V. A. Stephanovich, E. Ya. Sherman, N. T. Zinner, and O. V. Marchukov, Energy-level repulsion by spin-orbit coupling in two-dimensional Rydberg excitons, *Phys. Rev. B* **97**, 205407 (2018).
- [35] K. L. Lee, N. B. Jørgensen, L. J. Wacker, M. G. Skou, K. T. Skalmstang, J. J. Arlt, and N. P. Proukakis, Time-of-flight expansion of binary Bose-Einstein condensates at finite temperature, *New J. Phys.* **20**, 053004 (2018).
- [36] M. C. Gutzwiller, *Chaos in Classical and Quantum Mechanics* (Springer-Verlag, New York, 1990).